

## Chapter 2.8.3

# NEUTRON REFLECTION: PRINCIPLES AND EXAMPLES OF APPLICATIONS

**Robert Cubitt and Giovanna Fragneto**

Institut Laue-Langevin,  
6 rue Jules Horowitz,  
b.p. 156,  
F-38042 Grenoble,  
France

**SCATTERING IN MICROSCOPIC PHYSICS  
AND CHEMICAL PHYSICS**

**Neutron Scattering**

### Contents

§1	Introduction	1
§2	Theoretical Principles	2
	Absorption	4
	Magnetic Materials	4
	Roughness and Interdiffusion	4
§3	The Measurement of Neutron Reflection	5
	Data Analysis	6
§4	Examples of Applications	7
	Air/Solid Interface: Nickel Gratings	8
	Air/Liquid Interface: Detailed Structure of a Surfactant Monolayer	8
	Solid/Liquid Interface: The Structure of a New Model for Biological Membranes	9

## §1. Introduction

The reflection of light from surfaces is a well-known phenomenon caused by the change of refractive index across the interface. Already in 1675 Newton had realised that the colour of the light reflected by a thin film, illuminated by a parallel beam of white light, could be used to obtain a measure of the film thickness. Spectral colours develop as a result of interference between light reflected from the front and back surfaces of the film and optical interference is still used to measure the thickness of surface coatings. In the 1920s experiments by Compton showed that X-ray reflection was governed by the same laws as reflection of light but with different refractive indices depending on the number of electrons per unit volume. In 1944 Fermi and Zinn first demonstrated the mirror reflection of neutrons (Fermi and Zinn, 1946). Again this follows the same fundamental equations as optical reflectivity but with different refractive indices. Neutrons are scattered by nuclei and the neutron refractive index depends not only on the number of nuclei but also on how strongly they scatter. A quantity known as the scattering length that indicates a nucleus' ability to scatter neutrons may

be defined for each one. A neutron refractive index of any material is a function of the scattering length density of its constituent nuclei and the neutron wavelength. As with light, total reflection may occur when neutrons pass from a medium of higher refractive index to one of lower refractive index. Since the neutron refractive indices of most condensed phases are only slightly less than that of air or vacuum, total external reflection is more commonly observed instead of the total internal reflection experienced with light. The critical angle for total reflection is such that the reflectivity of neutrons of a given wavelength from a bulk interface is unity at lower glancing angles (ignoring absorption effects) and falls sharply at larger angles. Fermi and Zinn had observed the total reflection of thermal neutrons below the critical angle. Since the neutron refractive index is related to its composition and to the scattering lengths of its constituent atoms, measurement of the critical angle for total reflection for pure materials became an important method for the determination of the scattering lengths of nuclei. Indeed for a long time neutron reflection, besides being used in the transport of thermal neutron beams in guide tubes, has been used for such determinations even though the presence of interfacial inhomogeneity impaired the accuracy of the measurements. Over the past twenty years more accurate methods have been developed for measuring scattering lengths and neutron reflection has emerged as a powerful technique for investigating the inhomogeneities across the interface itself, inhomogeneities either in composition (Penfold and Thomas, 1990) or magnetisation (Felcher, 1981). As for light, interference occurs between waves reflected at the top and at the bottom of a film at an interface, which gives rise to interference fringes in the reflectivity profile.

For studies at interfaces neutron reflection offers many advantages with respect to traditional techniques as well as to X-ray reflection. In particular, because of the short wavelengths available, it has a resolution of a fraction of a nanometer, it is nondestructive and it can be applied to *buried*

interfaces, which are not easily accessible to other techniques. In addition it provides the advantage that isotopic substitution can be used to achieve large contrasts in the scattering length density. Information on the concentration profiles giving rise to the reflectivity curves is usually obtained through model fitting. Structure within a surface cannot be probed by specular reflection and off-specular studies become necessary (Sinha *et al.*, 1998). Much effort is being put recently in the optimisation of data analysis from off-specular measurements and in this direction are to be sought the future achievements of the technique as well as in new data analysis methods.

Neutron reflection is now being used for studies of surface chemistry (surfactants, polymers, lipids, proteins, and mixtures adsorbed at liquid/fluid and solid/fluid interfaces), surface magnetism (ultrathin Fe films, magnetic multilayers, superconductors) and solid films (Langmuir–Blodgett films, thin solid films, multilayers, polymer films).

After an introduction to the theory and measurement of neutron reflectivity, examples of applications at various interfaces will be given.

## §2. Theoretical Principles

In the quantum mechanical approach the neutron can be treated as a wave with a characteristic wavelength,  $\lambda$ , defined by the de Broglie relation,  $\lambda = h/m_n v$ , where  $h$  is Planck's constant, and  $m_n$  and  $v$  are the neutron mass and speed, respectively. The Schrödinger equation is analogous to the wave equation for light and leads to neutrons showing characteristic optical behaviour such as total reflection and refraction (Lekner, 1987; Sears, 1989). The Schrödinger equation may be written as

$$-\frac{\hbar^2}{8\pi^2 m_n} \nabla^2 \Psi + V \Psi = E \Psi, \quad (1)$$

where  $V$  is the potential to which the neutron is subject and  $E$  its energy.  $V$  represents the net effect of the interactions between the neutron and the scatterers in the medium through which it moves. Provided any scattering is far from satisfying the Bragg condition of the crystalline structure, the neutron can be considered to interact with a constant potential simply related to the coherent scattering length by the relation

$$V = \frac{\hbar^2}{2\pi m_n} N_b, \quad (2)$$

where  $N_b$  is the *scattering length density* defined as

$$N_b = \sum_j b_j n_j, \quad (3)$$

where  $n_j$  is the number of nuclei per unit volume and  $b_j$  is the scattering length of nucleus  $j$ . The latter is

an empirical quantity known for most nuclei, varying strongly across the periodic table and often varying sharply between isotopes of the same element. Most materials have a positive  $b$ ; therefore in a positive potential a neutron has less kinetic energy and hence a longer wavelength (opposite to light where the wavelength shortens).

We may now consider what happens to a beam approaching a surface with a bulk potential  $V$ , infinitely deep (see Fig. 1). With no structure within the surface the only potential gradient and hence force is perpendicular to the surface. Only the normal component of the incoming wave vector,  $k_i$  is altered by the barrier potential and it is the normal component of the kinetic energy  $E_{i\perp}$  that determines whether the neutron is totally reflected from the barrier,

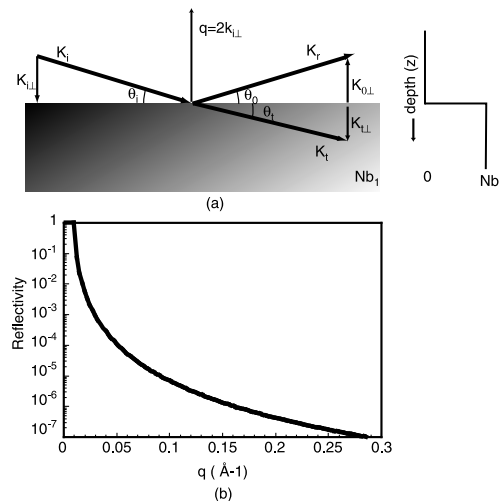
$$E_{i\perp} = \frac{(\hbar k_i \sin \theta_i)^2}{8\pi^2 m_n}, \quad (4)$$

where  $\theta_i$  is the angle of the incident beam. If  $E_{i\perp} < V$  then there is total reflection and the critical value of wave vector transfer,  $q_c$ , will be when  $E_{i\perp} = V$ , giving

$$q_c = \sqrt{16\pi N_b} \quad \text{as} \quad q = 2k_i \sin \theta_i. \quad (5)$$

Assuming the interaction is elastic, then conservation of momentum means that  $\theta_i = \theta_o$  where  $\theta_o$  is the angle of the reflected beam; i.e., the reflection is specular. Provided the sample is static, any off specular reflection must be a result of potential gradients within the  $xy$  plane of the surface.

**Figure 1** (a) Reflection of an incident beam from an ideally flat interface.  $k_i$  and  $k_r$  are the incident and scattered wave vectors, with angles  $\theta_i = \theta_o = \theta$  in the incidence plane;  $q$  is the wave vector transfer; and  $N_{b1}$  is the scattering length density of the semi-infinite substrate. On the right is the scattering length density profile as a function of depth. (b) Simulation of the specular neutron reflectivity as a function of  $q$  from a silicon/air interface ( $N_{b1} = 2.07 \times 10^{-6} \text{ \AA}^{-2}$ ).



If  $E_{i\perp} > V$ , then the reflection is not total and the neutron can be either reflected or transmitted into the bulk of the material. The transmitted beam,  $k_t$ , with its normal component of kinetic energy reduced by the potential must change direction; i.e., it is refracted. The change in the normal wave vector is

$$k_{t\perp}^2 = k_{i\perp}^2 - 4\pi N_b, \quad (6)$$

allowing us to define a refractive index  $n$

$$n^2 = \frac{k_t^2}{k_i^2} = \frac{k_{i\parallel}^2 + (k_{i\perp}^2 - 4\pi N_b)}{k_i^2} = 1 - \frac{4\pi N_b}{k_i^2} = 1 - \frac{\lambda^2 N_b}{\pi}, \quad (7)$$

where  $\lambda$  is the neutron wavelength. For most materials,  $N_b$  is much less than 1, so for  $\lambda < 60 \text{ \AA}$  we can make a good approximation for  $n$  with the well-known result

$$n \approx 1 - \frac{\lambda^2 N_b}{2\pi}. \quad (8)$$

This confirms the earlier statement about the wavelength change in the bulk being opposite to that of light (for positive  $b$ ) as we see that  $n$  is less than 1. The transmitted beam refracts towards the mirror plane and exactly at the point of total reflection, the refracted beam travels along the surface.

All of the above discussion (apart from treating neutrons as waves) can be derived from classical physics. In order to describe all the physical aspects of reflectometry a quantum mechanical approach must be used. The wavefunction describing the probability amplitude of a neutron near to the surface is

$$\frac{\partial^2 \Psi_z}{\partial z^2} + k_{\perp}^2 = 0, \quad \text{where} \quad k_{\perp}^2 = \frac{2m_n}{\hbar^2} (E_i - V) - k_{\parallel}^2. \quad (9)$$

Solutions for this above and below the surface are

$$\Psi_z = e^{ik_{i\perp}z} + r e^{-ik_{i\perp}z} \quad \text{and} \quad Y_z = t e^{ik_{t\perp}z}, \quad (10)$$

where  $r$  and  $t$  are the probability amplitudes for reflection and transmission. Continuity of the wavefunction and its derivative gives the expressions

$$1 + r = t \quad k_{i\perp} (1 - r) = t k_{t\perp}, \quad (11)$$

where the second relation only holds for  $E_{i\perp} > V$ ; this leads directly to the classical Fresnel coefficients found in optics:

$$r = \frac{k_{i\perp} - k_{t\perp}}{k_{i\perp} + k_{t\perp}} \quad \text{and} \quad t = \frac{2k_{i\perp}}{k_{i\perp} + k_{t\perp}}. \quad (12)$$

In reflectometry the reflectivity is measured as a function of wave vector transfer or  $q$ . Using the expressions (5), (6) and (12) the measured reflectivity  $R$  can

be related to  $q$  and  $q_c$ . Note that what is measured is an intensity and thus is a function of the quantum mechanical probability amplitude squared.

$$R = r^2 = \left[ \frac{q - (q^2 - q_c^2)^{1/2}}{q + (q^2 - q_c^2)^{1/2}} \right]^2. \quad (13)$$

When  $q \gg q_c$  this reduces to

$$R \approx \frac{16\pi^2}{q^4} N_b^2, \quad (14)$$

which is the reflectivity used in the Born approximation (Born and Wolfe, 1989).

Returning to the wavefunction within the surface (10) and using (6) it is found that when  $E_{i\perp} < V$  (or  $k_{i\perp}^2 < 4\pi N_b$  or  $q < q_c$ ) there is a real solution of the form

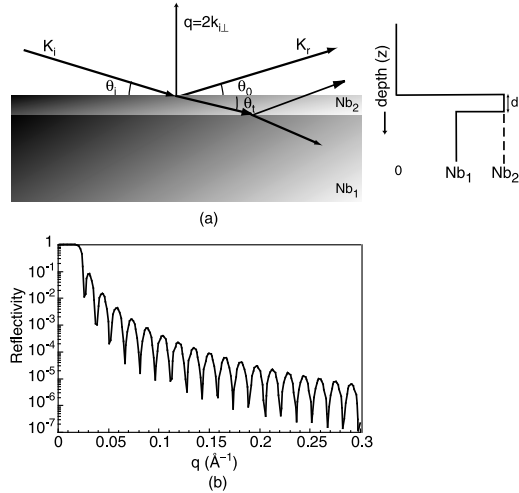
$$Y_z = t e^{i(k_{i\perp}^2 - 4\pi N_b)^{1/2} z} = t e^{-\frac{1}{2}(q_c^2 - q^2)^{1/2} z}. \quad (15)$$

This is a very important result as it shows that even when the potential barrier is higher than the particle energy normal to the surface it can still penetrate to a characteristic depth of  $(q_c^2 - q^2)^{-1/2}$ . This “evanescent” wave travels along the surface with wave vector  $k_{\parallel}$  and after a very short time it is ejected out of the bulk in the specular direction (see Fig. 2a). Taking as example the value of  $N_b$  for Si this penetration is on the order of  $100 \text{ \AA}$  at  $q = 0$ , rising rapidly to infinity at  $q = q_c$ . No conservation laws are broken, as the reflectivity is still unity due to the fact that this wave represents no flux transmitted into the bulk. The result also explains why when a thin layer of material such as Ni, which has a much larger  $N_b$ , is put onto a Si substrate  $q_c$  is still defined by the  $N_b$  of Si and not of Ni. The reason being in this case the layer is thinner than the characteristic penetration depth and the neutrons tunnel through the barrier.

Calculating the reflectivity from such a system or one with many layers requires a general technique such as the optical matrix method (Born and Wolfe, 1989). The transmission and reflection from one layer to the next can be described as a matrix multiplication product for each layer. The problem of inverting a reflectivity curve to extract  $N_b$  as a function of depth is complex and many profiles can produce the same reflectivity curve (this is known as the *phase problem*). In Fig. 2b is an example of reflectivity profile associated with a single layer of the form in Fig. 2a with  $d = 400 \text{ \AA}$ . In the Born approximation these oscillations are simply the Fourier transform squared of  $N_b$  as a function of depth multiplied by the Fresnel reflectivity, the period of which at  $q \gg q_c$  is  $2\pi/d$ .

A useful review of the various techniques for inversion can be found in Zhou and Chen (1995).

**Figure 2** (a) As described in the legend to Fig. 1a with an additional thin layer of scattering length density  $N_{b2}$ . (b) Simulation of the specular neutron reflectivity as a function of  $q$  from a 400-Å layer of nickel on a silicon substrate ( $N_{b1} = 2.07 \times 10^{-6} \text{ \AA}^{-2}$ ,  $N_{b2} = 9.04 \times 10^{-6} \text{ \AA}^{-2}$ ).



### Absorption

In reality many materials have a finite absorption cross section, although for most materials absorption does not significantly reduce the reflectivity. This is dealt with by adding an imaginary part to the coherent scattering length:

$$b_{\text{total}} = b_{\text{coherent}} + ib_{\text{absorption}}. \quad (16)$$

It can be seen then from (10) that the transmitted and the reflected intensity is exponentially reduced by the presence of absorption. Even in the regime of total reflection, as the evanescent wave exists in a surface region of the material, absorption occurs, reducing the total reflection amplitude to less than 1. It should not be forgotten that even materials such as Cd and Gd, which are very strong absorbers of neutrons, can still have significant reflectivities.

### Magnetic Materials

We have seen that a neutron in the bulk is affected by a mean potential related to the coherent scattering length. If the material is magnetised, then there is an additional potential associated with the interaction of the magnetic dipole moment of the neutron and magnetic flux density  $B$ . This potential has the value

$$V_{\text{mag}} = -\boldsymbol{\mu} \cdot \mathbf{B}(r), \quad (17)$$

where  $\boldsymbol{\mu}$  is the magnetic dipole moment of the neutron and  $\mathbf{B}(r)$  is the spatially varying magnetic field. If the incoming beam is polarised up or down with respect to the magnetisation of the sample then the magnetic

potential switches sign. The magnetic potential can be expressed in the form of a coherent scattering length

$$b_m = 1.913 \frac{e^2}{m_e} S, \quad (18)$$

where  $e$  and  $m_e$  are the electron charge and mass, respectively and  $S$  is the effective spin of the magnetic atom perpendicular to the momentum transfer of the reflection. The total coherent scattering length becomes polarisation dependent with the plus sign corresponding to a beam polarised by a polariser with a magnetisation in the same direction as the magnetisation of the sample:

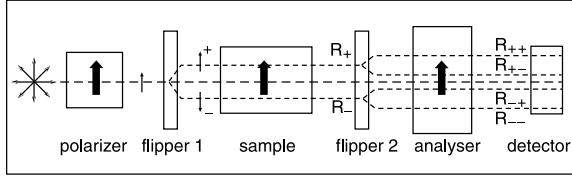
$$b_{\text{total}} = b_{\text{nuclear}} \pm b_m. \quad (19)$$

Assuming the sample is a saturated ferro-magnet, to extract the nuclear and magnetic parts of  $b$ , two measurements must be made, one with the polarisation parallel to the magnetisation,  $R_+$ , and the other with the polarisation inverted,  $R_-$ , by use of a flipper (Williams, 1989). A very important point in polarised neutron reflectometry (PNR) is to remember that magnetic reflection is only going to occur at a potential boundary and that requires a step in  $B$ . If a sample has been magnetised within the plane of a magnetic layer, then, from Maxwell's equations, the step in  $B$  is  $\mu_0 M$  at the surface, where  $M$  is the magnetisation density of the layer. If the sample is magnetised normal to the plane, then  $B$  is continuous at the boundary and there is no potential step. Magnetic reflection can only occur in the presence of in-plane magnetisation components. Components of magnetisation normal to the plane do not reflect an in-plane polarised beam but can cause spin flip; i.e., a completely polarised beam will have a certain fraction polarised in the opposite direction after reflection. This can only be measured by the use of a second flipper and polariser or analyser. Figure 3 shows the four combinations of the initial and final polarisation states needed to measure the four reflectivities, i.e.,  $R_{++}$ ,  $R_{--}$ ,  $R_{+-}$ ,  $R_{-+}$ . It should be noted that from the polariser to the analyser there must be a small vertical guide field that maintains the polarisation direction. In addition to measuring these four reflectivities the four cases should also be measured with a nonmagnetic scatterer such as graphite to enable the imperfection of the flipper and polariser efficiencies to be taken into account. A detailed description of neutron optics and magnetic effects can be found in Williams (1989).

### Roughness and Interdiffusion

There is a large field of interest in what happens between materials at an intermaterial boundary. An interface may be rough with peaks and troughs over

**Figure 3** A schematic layout of a polarised neutron reflectivity experiment with analysis. The initially unpolarised beam is polarised vertically by the polariser mirror. Flipper 1, when activated, inverses the polarisation, allowing the measurement of  $R_+$  and  $R_-$ . The difference of these two data sets represents the magnetic contribution to the reflectivity. If in the process of reflection the neutron polarisation was changed (flipped) due to a magnetisation component out of the vertical plane, this can be detected by the use of an analyser mirror and second flipper. Between the polariser and analyser a guide field ( $\sim 20$  G) is required to maintain the polarisation in the vertical direction.

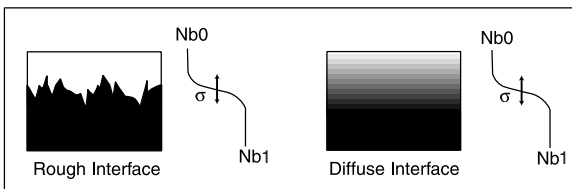


a large range of length scales with a fractal-like structure. It may also have magnetic roughness if the magnetisation does not sharply change at an interface. A boundary may be smooth but with one material diffused into the other. It turns out that in both the rough and diffuse cases the specular reflectivity is reduced by a factor very much like the Debye–Waller factor reduces scattered intensity from a crystal (Nénot and Croce, 1990). The resulting density profiles are the same, as shown in Fig. 4. Expression (14) is affected in the manner

$$R \approx \left( \frac{16\pi^2}{q^4} N_b^2 \right) e^{-q_z^2 \sigma^2}, \quad (20)$$

where  $\sigma$  is a characteristic length scale of the layer imperfection. So what happens to the intensity lost by the exponential factor in (20)? In the case of the diffuse interface the lost intensity must go into the transmitted beam as there are no potential gradients in any other direction than normal to the surface. This is not the case for the rough interface where intensity is lost by local reflections in directions away from the specular direction or off-specular scattering. Information such as the height–height correlation function can be deduced from this off-specular scattering (Born

**Figure 4** Two possible interfaces that can result in identical specular reflectivities. The data only differ in the case of the rough interface where off-specular scattering is observed.



and Wolfe, 1989; Daillant and Gibaud, 1999). If the in-plane structure is regular as in an optical grating then the off-specular can be quite dramatic, see example 4.1.

### §3. The Measurement of Neutron Reflection

The basic features of a reflection experiment, whether this uses light, X-rays or neutrons are (i) a radiation source, (ii) a wavelength selector or chopper(s), (iii) a system of collimation, (iv) the sample and (v) a detection system.

The production of neutrons requires either a nuclear reactor, where a continuous neutron beam is produced by nuclear fission, or a synchrotron source, where a pulsed neutron beam is obtained. In both cases neutron energies are too high for large-scale ( $> 100 \text{ \AA}$ ) structural studies and are reduced in a moderator tank (e.g.,  $D_2$  at 25 K) where the neutrons are repeatedly scattered, losing energy at each collision until thermal equilibrium is reached. Thermal neutron energies are on the order of  $k_B T$ , where  $T$  is the temperature of the water moderator and  $k_B$  the Boltzmann constant.

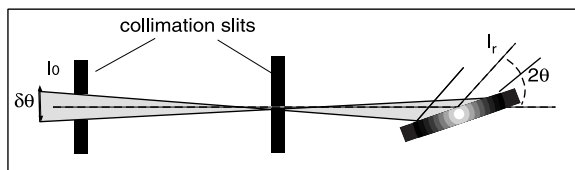
The objective of a specular neutron reflection experiment is to measure the reflectivity as a function of the wave vector perpendicular to the reflecting surface,  $q$ . The measurement can be done by varying either the glancing angle of incidence  $\theta$  at constant wavelength or measuring the time-of-flight, hence wavelength, at constant  $\theta$ . In most nuclear reactors measurements are usually made at a fixed value of  $\lambda$  using long-wavelength neutrons ( $\sim 10 \text{ \AA}$ ) and a  $\theta$  (reflection angle)  $-2\theta$  (detector angle) scan. Wavelength selection may be achieved by Bragg scattering from a crystal monochromator or multilayer or by velocity selection through a mechanical device. The incoming intensity must also be measured either at the same time with the use of a monitor and then scaled up by the monitor efficiency or in the separate experiment. The reflectivity is simply the ratio of these two intensities for each  $\theta$ , which is converted to  $q$  by Bragg's law:

$$q = 4\pi \sin(\theta) / \lambda. \quad (21)$$

With a sample length on the order of a few centimeters and a starting  $\theta$  of a fraction of a degree, the beam must be finely collimated to ensure the sample is not overilluminated; i.e., all of the incoming beam strikes the reflection surface (see Fig. 5). The sample can be overilluminated for very small samples but the data must be corrected for the varying flux on the sample as  $\theta$  is increased.

As the reflectivity tends to drop quite fast with increasing  $q$  (see (14) where  $R \propto 1/q^4$ ) in order to gain intensity (at the price of looser resolution) the

**Figure 5** A typical collimation setup within the reflection plane. When the sample is underilluminated (minimal background), the distance between the last slit and the sample should be as short as possible. In general the divergence out of the plane is defined only by the source.



collimation slits can be opened, keeping  $\delta\theta/\theta$  constant and equal to the fractional wavelength variation. The final curve in either case must have the resultant  $q$  resolution,  $\delta q$ , deconvolved from the data. The  $q$  resolution is related to  $\theta$  and  $\lambda$  by the relation

$$\left(\frac{\delta q}{q}\right)^2 = \left(\frac{\delta\theta}{\theta}\right)^2 + \left(\frac{\delta\lambda}{\lambda}\right)^2. \quad (22)$$

This method has the advantage that the wavelength chosen can be that with the highest flux from the neutron source and therefore for a given resolution is the most efficient method of using the flux available.

The alternative is to use time-of-flight (TOF), which is used at both spallation and reactor sources.  $\theta$  is kept constant and all the available wavelengths in the beam are used. The wavelength and hence  $q$  are measured by pulsing the incoming beam and measuring the arrival time to the detector. The resolution is the same as (22) with  $\delta\lambda/\lambda$  replaced by  $\delta t/t$ , where  $\delta t$  is the pulse time width and  $t$  is the time-of-flight of the pulse. The resolution of the time binning at the detector in principle is also a factor but in practice this is chosen to be much smaller than  $\delta t$ . The range of  $q$  covered for a given  $\theta$  depends on the useful wavelength range. Over this range however, the flux at the minimum and maximum wavelengths compared to the peak flux may be more than two orders of magnitude smaller. The highest  $q$  (and lowest reflectivity) is measured by the shortest wavelength. For the same resolution the TOF method is less efficient than the monochromatic technique as it will always require longer counting times to measure the same  $q$  range to the same statistical accuracy. Nevertheless, kinetic experiments are best done in the TOF mode. If one had a sample where the layer structure was changing as a function of time, only the TOF method can produce a unique  $R(q)$  for a given time range. The  $\theta-2\theta$  measurement is a sequential set of counts so each point in  $q$  is measured at a different time. In order to solve the problem of reduced flux in TOF, a chopper system can continuously vary the time resolution (see <http://www.ill.fr/Yellowbook/D17/main.html>) Figure 6 is a schematic representation of a reflectometer.

At high values of  $q$  the reflectivity is very small and most of the beam passes into the substrate (e.g., water in a solid/liquid experiment) where it is scattered either incoherently or by multiple diffraction. A proportion of this scattering enters the detector with the specular reflection and contributes a background, which must be subtracted from the profile. This defines a lower limit of reflectivity that can be measured, which is on the order of  $10^{-7}$  when water is present in the sample environment.

With a two-dimensional multidetector a wide range of  $2\theta$ , which will include background and off-specular diffraction, is captured. Instruments with a single detector require a special measurement with the detector in an off-specular position to measure the background. In both cases care must be taken in deciding the  $2\theta$  range for background does not include diffracted intensity from the sample itself.

Polarised neutron reflection (PNR) experiments are complicated by the fact that the polarisers and flippers in the system are not perfect. With no sample and incoming beam directly on the analyser we would expect no flux on the detector in the condition  $-+$  or  $+ -$  for a perfect system. A measure of the efficiency of each flipper and the polarisers is the flipping ratio  $F$  defined as

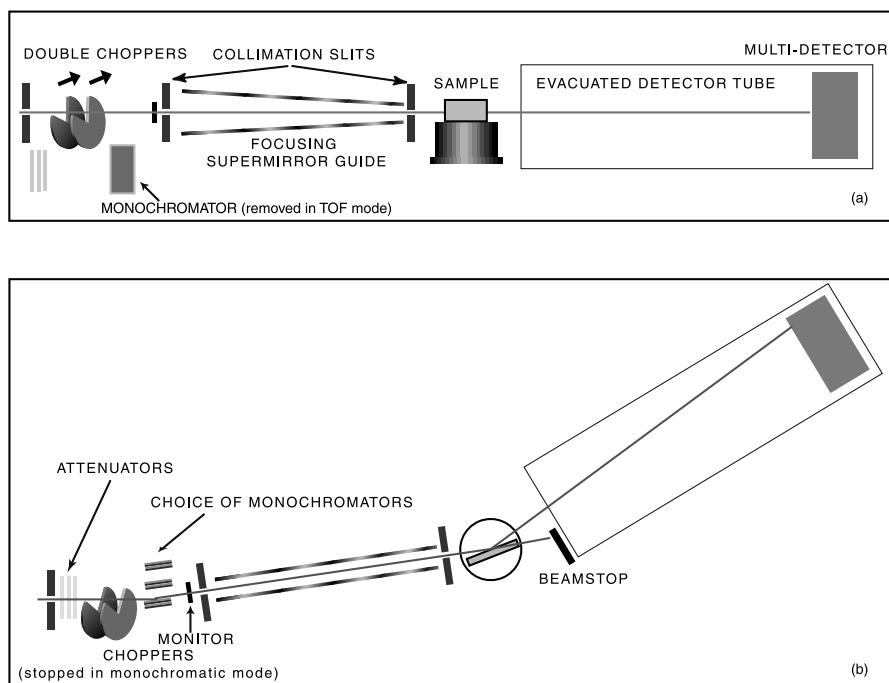
$$F_1 = I_{++}/I_{-+} \quad \text{and} \quad F_2 = I_{+-}/I_{--}, \quad (23)$$

where  $F_1$  and  $F_2$  are the flipping ratios for the first and second flippers. The intensities are measured either with the direct beam for a single detector or with a sample such as graphite in which the scattering is entirely non-spin-flip in order to measure the analyser/flipper efficiency over a range of  $2\theta$ . The measured intensities,  $I$ , correspond to the states of the two flippers as in Fig. 3. Acceptable flipping ratios are on the order of 40. These must be taken into account when attempting to extract the magnetic and nuclear components of the reflectivity (Williams, 1989).

### Data Analysis

The method of analysis often used for specular reflection data involves the construction of a model of the interface that may be represented by a series of parallel layers of homogeneous material. Each layer is characterised by a scattering length density,  $\rho$ , and a thickness,  $d$ , which are used to calculate a model reflectivity profile by means of the optical matrix method. The interfacial roughness between any two consecutive layers,  $\sigma$ , may also be included in the model by the Abeles method (Heavens, 1955). The calculated profile is compared to the measured profile and the quality of the fit is assessed either visually or by using  $\chi^2$  in the least-squares method (the two extremes of the interface are considered as having

**Figure 6** The dual mode instrument D17 at the ILL designed to take advantage of both TOF and monochromatic methods of measuring reflectivity. (a) A side view of the instrument in TOF mode. The monochromator is removed from the beam and a double-chopper system defines the time resolution ( $1\text{--}20\% \delta t/t$ ). Between the collimation slits is a vertically focussing guide that increases the flux at the sample position at the price of increased vertical divergence of the beam. The slits define the beam in the horizontal direction. (b) A vertical view of the instrument in monochromatic mode. Here the collimation arm is rotated ( $\sim 4^\circ$ ) to allow the beam reflected from the multilayer monochromator system to pass through to the sample. The choice of monochromators involves high and low resolution ( $2\text{--}5\%$ ) plus polarising.



infinite thickness and have a fixed scattering length density). At the interface there is either a single uniform layer or a more complicated structure. By variation of  $\rho$  and  $d$  for each layer, the calculated profile may be compared with the measured profile until the optimum fit to the data is found. Although any one profile may not provide a unique solution, the use of different isotopic contrasts together with the physical and chemical constraints of the system can usually ensure that an unambiguous model of the interface is obtained. *Contrast variation* relies on the fact that the different nuclei scatter neutrons with different amplitude, and sometimes, as in the case of protons and deuterons, with oppositely signed scattering lengths ( $N_b^{\text{H}_2\text{O}} = -0.56 \times 10^{-6} \text{ \AA}^{-2}$ ;  $N_b^{\text{D}_2\text{O}} = 6.35 \times 10^{-6} \text{ \AA}^{-2}$ ). By using a combination of hydrogenated and deuterated materials the reflectivity profile of a system can be substantially changed while keeping the same chemical structure at the interface. It is also possible, by adjustment of the H/D ratio, to prepare solvents that are contrast matched to the medium through which neutrons pass before reaching the interface, that is, the bulk solid in a solid/fluid experiment or air in a liquid/air experiment. The contrast

between the solid (or air) and the solvent is then zero, giving a reflectivity profile arising only from the interfacial region. From the value of the scattering length density of the layer, information about its composition is obtained. The kinematic approximation (Crowley, 1993) gives a more direct description of the structure of soluble surfactant monolayers at the air/liquid interface. Very recently, Majkrzak *et al.* (2000) have succeeded in applying a new, phase-sensitive method for revealing compositional depth profiles. With this method the scattering length density profile of biomimetic membranes is obtained by a first principles inversion without the need for fitting or adjustable parameters. Other model-free approaches use maximum entropy (Silvia *et al.*, 1991) and B-splines (Berk and Majkrzak, 1991).

#### §4. Examples of Applications

Neutron specular reflection has been applied to several systems including magnetic multilayers (Huang *et al.*, 1991; Schreyer *et al.*, 1995; Majkrzak, 1996), polymers (Daillant and Gibaud, 1999, and references therein), surfactants (Penfold *et al.*, 1997, and references therein) and proteins (Lu and Thomas, 1998,

and references therein) at various interfaces. The liquid/liquid interface deserves a special mention for its technological importance as well as its fundamental interest. Interesting work has been done recently from a phospholipid monolayer at a flat water/oil interface by using synchrotron radiation (Fradin *et al.*, 1998). It is more difficult to use neutrons since when the beam crosses one of the two liquid phases to reach the interface, absorption lowers considerably the signal. Nevertheless, the optimisation of sample preparation and data collection protocols could lead to useful results in the near future.

Below are three randomly selected examples of results from various interfaces that give a flavour of what may be attained by this technique.

#### Air/Solid Interface: Nickel Gratings

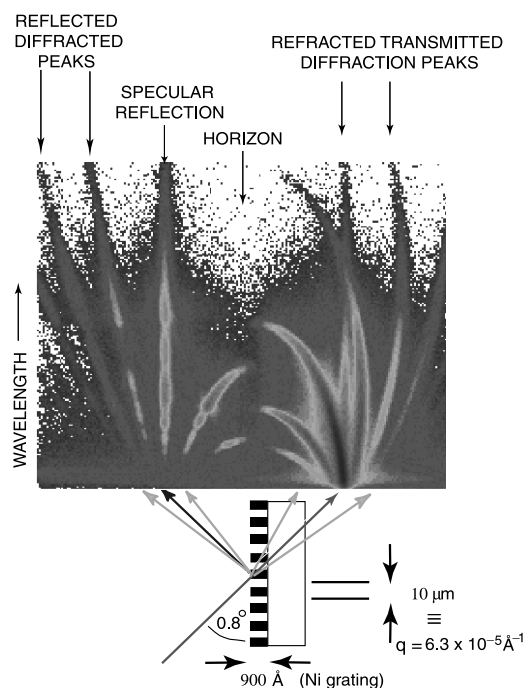
About the specular reflection there can be off-specular scattering arising from surface roughness or as in the case described below, low-angle diffraction. The sample was a diffraction grating consisting of a glass substrate with thousands of strips of nickel, 900 Å deep separated by 10 μm (Cubbitt, 2000; Ott *et al.*, 2000). If this grating were placed perpendicular to the incoming beam, then 10-Å neutrons would be diffracted only a few thousandths of a degree ( $q_x = 6 \times 10^{-5} \text{ \AA}^{-1}$ ), beyond the range of any existing small-angle instrument. However, if the incoming beam strikes the grating surface at a glancing angle, then many diffraction orders can be seen in both the reflected and transmitted beams at measurable angles of deflection (Fig. 7). In addition to information on the stripe separation, the depth profile (consistent with 900 Å) is revealed in the ripples of intensity found running along the specular line and the various reflected diffraction orders. The diagonal line of intensity coming from where the specular line just totally reflects is a Yoneda wing and is a consequence of the roughness along the surface of the nickel strips.

These devices may have application as monochromators or wavelength analysers.

#### Air/Liquid Interface: Detailed Structure of a Surfactant Monolayer

Amphiphiles are a class of molecules exhibiting a strong tendency to adsorb at interfaces. They are characterised by the presence of both polar (hydrophilic) and nonpolar (hydrophobic) moieties. Surfactants (surface-active agents) are amphiphiles and typically have a long hydrophobic chain, known as tail, and a small hydrophilic group, known as head. At interfaces, the molecule can be oriented in different ways and in general the hydrophilic head is directed towards the bulk water and chains will orient in

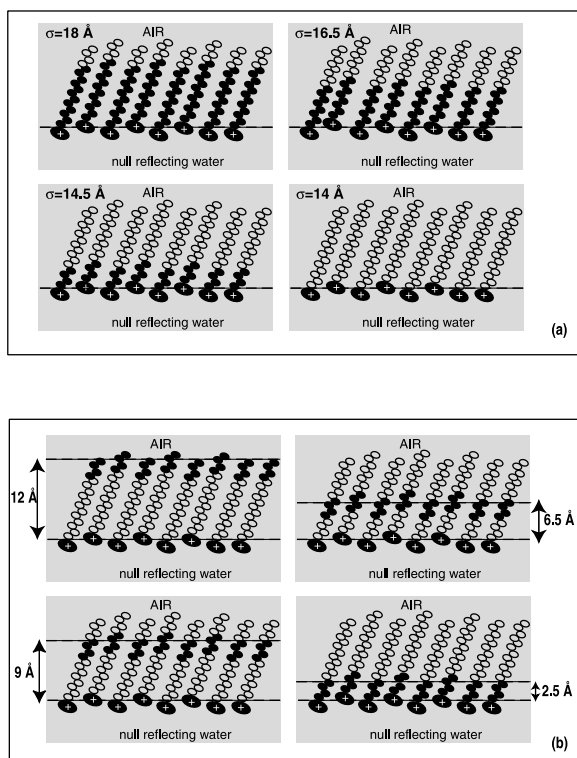
**Figure 7** TOF data showing reflection, refraction and off-specular diffraction from a nickel grating on a glass substrate measured on D17. The horizontal axis is  $x$  pixels of the detector ( $\propto 2\theta$ ) summed over the vertical direction. The vertical axis is TOF ( $\propto \lambda$ ).



order to avoid the water. The structure of surfactants in bulk solution and at interfaces is of great importance in industrial processes involving, for example, detergency, paints, food chemistry and oil recovery. Much successful work has been done to understand the structure of surfactant aggregates in solution but at interfaces a systematic study of the effects of the nature and composition of a surfactant on the properties of adsorbed layers is still lacking. Neutron reflection, combined with H/D isotopic substitution, is an ideally suited technique for this kind of study as it makes it possible to determine the position of the molecules at the interface in relation to the aqueous subphase and the relative position of the hydrophilic and hydrophobic groups. In the following example it is shown how, by suitable use of deuterium-labelled materials, the three basic pieces of information, surfactant thickness, the depth the surfactant penetrates into water and the surface coverage of a surfactant monolayer, were derived from specular neutron reflection measurements (Lu *et al.*, 1995).

The method has been applied to the surfactant hexadecyltrimethylammonium bromide (CTAB), whose hydrocarbon chain is 16 atoms long. First it was labelled with deuterium to give a series of compounds with 4, 8, 12 and 16 CD<sub>2</sub> groups. Specular reflectivity measurements were then taken in null reflecting

**Figure 8** Cartoon of the results from neutron specular reflectivity experiments from CTAB monolayers at the air/water interface. By using null reflecting water ( $\sim 86\%$  H<sub>2</sub>O and 14% D<sub>2</sub>O) and differently labelled carbons in the surfactant hydrocarbon chains fine details of the interface are revealed. (a) Filled circles are deuterated CD<sub>2</sub> groups, empty circles are hydrogenated CH<sub>2</sub> groups;  $\sigma$  is the layer roughness as obtained from kinematic approximation data analysis (Crowley, 1993). (b) Scheme of labelling that makes it possible to obtain the mean conformation of the hydrocarbon chain. Adapted from Lu *et al.* (1995).



water, that is, a mixture of H<sub>2</sub>O and D<sub>2</sub>O with the same scattering length density as air. In this way the deuterated parts of the interface were highlighted (see Fig. 8a). The thicknesses of this series of compounds could then be used to show that there is a large residual roughness of the layer of  $14 \text{ \AA}$ . This is obtained by plotting the measured thickness of the layer against the number of labelled carbons and extrapolating to zero length of the label. By making the same surfactant with different pairs of deuterium-labelled butylene groups (four carbon atoms) the mean vertical separation between the labels was determined (see Fig. 8b). Making the further assumption that each four-carbon fragment is on average fully extended, the mean conformation of the carbon chain may be deduced. This series of measurements showed that the surfactant layer must be highly disordered, the roughness being comparable with the projection of the chain along the surface normal, a result that agrees with computer simulations.

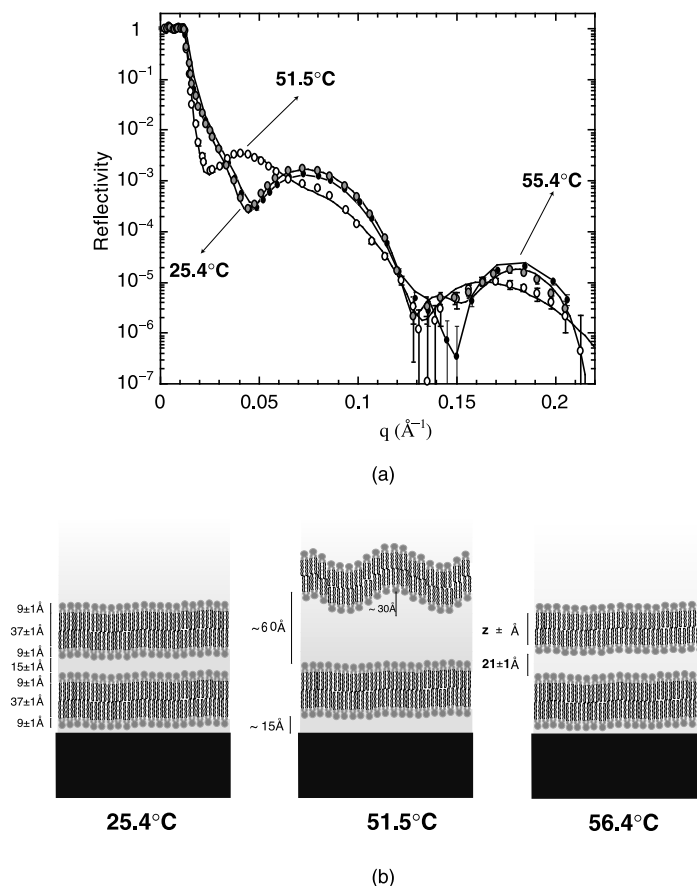
### Solid/Liquid Interface: The Structure of a New Model for Biological Membranes

Lipid bilayers are the basic building units of biological membranes. Many biological processes involve transformations between such bilayer structures. Several model membrane systems have been developed for studying the properties of pure lipids, lipid mixtures and lipid-protein mixtures and they can be grouped as (i) monolayers, (ii) planar bilayers and (iii) liposomes or vesicles. Phospholipid bilayers have been intensely used as model systems for studying the structure and interactions of biological membranes. Very recently a new model system has been produced, consisting of two bilayers, one adsorbed on a flat surface and a second floating at 15 to 30  $\text{\AA}$  above the first in bulk water. A cartoon of this system is depicted in Fig. 9b. The floating bilayer at the solid-liquid interface is a new model for biological membranes with several advantages over classical model systems (Charitat *et al.*, 1999; Fragneto *et al.*, 2000). Below, a study of the behaviour of this system when varying the temperature is briefly discussed.

Phospholipid bilayers exhibit a main phase transition from a gel phase, where lipid chains are rigid and well ordered, to a liquid crystalline phase ( $L_{\alpha}$ ), where chains are disordered and fluid-like. Cell membranes are in the fluid state. The two bilayers are best deposited in the gel phase. After deposition the temperature of the system may be raised in order to overcome the gel-fluid phase transition. Neutron specular reflectivity measurements make it possible to conclude that the bilayer is stable well above the main transition temperature (in the biologically relevant fluid phase) and that at the transition both the interbilayer distance and the roughness increase. Figure 9a shows the neutron reflectivity measurements from hydrogenated di-stearyl phosphatidyl choline (DSPC) in D<sub>2</sub>O at 25.4°C (gel phase), 51.5°C (around the main phase transition) and 55.4°C (fluid phase). It may be observed already from the reflectivity profiles that at 51.5°C the thickness of the system increases since the position of the first minimum shifts towards a lower  $q$  value. In the fluid phase the profile is very similar to that in the gel phase, indicating that there are no major changes in the structure in the direction normal to the interface.

Data were fitted with a box model and reflectivity was determined with the optical matrix method (continuous lines in Fig. 9a). Results are summarised in the cartoon of Fig. 9b and they indicate that at 51.5°C not only does the interbilayer distance increase enormously but so does the floating bilayer roughness. This might be a direct observation of the balance between energy minimisation and entropy repulsion, leading to an estimation of the membrane bending

**Figure 9** (a) Neutron reflectivity profiles and fitted curves (continuous lines) from DSPC phospholipid bilayers at the silicon/water interface; data were collected on the diffractometer D16 at the ILL. (b) Cartoon of the model used to fit the data. Adapted from Fragneto *et al.* (2000).



modulus in the two lipid phases as well as at the transition.

## References

- Berk, N. F. and Majkrzak, C. F. 1991, *Phys. Rev. B* **51**, 11,296.
- Born, M. and Wolfe, E. 1989, In *Principles of Optics*, Pergamon Press, Oxford.
- Charitat, T., Bellet-Amalric, E., Fragneto, G. and Graner, F. 1999, *Eur. Phys. J. B* **8**, 583.
- Crowley, T. L. 1993, *Physica A* **195**, 354.
- Cubitt, R. 2000, *ILL Annual Report*.
- Daillant, J. and Gibaud, A. 1999, In *X-ray and Neutron Reflectivity: Principles and Applications*, Springer-Verlag, Berlin.
- Felcher, G. P. 1981, *Phys. Rev. B* **24**, 1995.
- Fermi, E. and Zinn, W. H. 1946, *Phys. Rev.* **70**, 103.
- Fradin, C., Luzet, D., Braslau, A., Alba, M., Daillant, J., Petit, J. M. and Rieutord, F. 1998, *Langmuir* **14**, 7329.
- Fragneto, G., Charitat, T., Graner, F., Mecke, F. T., Perino-Gallice, L. and Bellet-Amalric, E. 2000, *Europhys. Lett.* **53**, 100–106.
- Heavens, O. S. 1955, In *Optical Properties of Thin Films*, Butterworths, London.
- Huang, Y. Y., Felcher, G. P. and Parkin, S. S. P. 1991, *J. Magn. Magn. Mater.* **99**, 31.
- Lekner, J. 1987, In *Theory of Reflection*, Martinus Nijhoff, Dordrecht.
- Lu, J. R. and Thomas, R. K. 1998, *J. Chem. Soc. Faraday Trans.* **94**, 995.
- Lu, J. R., Li, Z. X., Smallwood, J., and Thomas, R. K. 1995, *J. Phys. Chem.* **99**, 8233.
- Majkrzak, C. F. 1996, *Physica B* **221**, 342.
- Majkrzak, C. F., Berk, N. F., Krueger, S., Dura, J. A., Tarek, M., Tobias, D., Silin, V., Meuse, C. W., Woodward, J. and Plant, A. 2000, *Biophys. J.* **79**, 3330.
- Nénot, L. and Croce, P. 1990, *Rev. Phys. Appl.* **15**, 761.
- Ott, F., Menelle, A., Fermon, C. and Humbert, P. 2000, *Physica B* **283**, 418.

- Penfold, J. and Thomas, R. K. 1990, *J. Phys. Condens. Matter* **2**, 1369.
- Penfold, J., Richardson, R. M., Zarbakhsh, A., Webster, J. R. P., Bucknall, D. G., Rennie, A. R., Jones, R. A. L., Cosgrove, T., Thomas, R. K. and Higgins, J. S. 1997, *J. Chem. Soc. Faraday Trans.* **93**, 3899.
- Schreyer, A., Ankner, J. F., Zeidler, T., Zabel, H., Majkrzak, C. F., Schaefer, M. and Gruenberg, P. 1995, *Euro. Phys. Lett.* **595**.
- Sears, V. F. 1989, *Neutron Optics*, Oxford Univ. Press, Oxford.
- Silvia, D. S., Hamilton, W. A. and Smith, G. S. 1991, *Physica B* **173**, 121.
- Sinha, S. K., Sirota, E. B., Garoff, S. and Stanley, H. B. 1998, *Phys. Rev. B* **38**, 2297.
- Williams, W. 1989, *Polarized Neutrons*, Oxford Univ. Press, Oxford.
- Zhou, X.-L. and Chen, S.-H. 1995, *Phys. Rep.* **257**, 223.